Article

Insights into the Relationship between Crystallite Size, Sintering Pressure, Temperature Sensitivity, and Persistent Luminescence Color of Gd$_{2.97}$Pr$_{0.03}$Ga$_3$Al$_2$O$_{12}$ Powders and Ceramics

Paweł Głuchowski,* Robert Tomala, Daniela Kujawa, Vitalii Boiko, Tomas Murauskas, and Piotr Solarz

Read Online

ACCESS | Metrics & More | Article Recommendations | SI Supporting Information

ABSTRACT: In order to obtain Gd$_{2.97}$Pr$_{0.03}$Ga$_3$Al$_2$O$_{12}$ powders with different crystallite sizes, a modified Pechini (sol−gel) method was used. Powders were then used for the preparation of ceramics by a high-pressure low-temperature sintering method. The impact of crystallite size and pressure applied during the sintering procedure on conventional and persistent luminescence was investigated and analyzed. It was found that the emission color is strictly dependent on the crystallite size, as such phenomenon may be used in the field of advanced anti-counterfeiting. The spectroscopic properties of Gd$_{2.97}$Pr$_{0.03}$Ga$_3$Al$_2$O$_{12}$ were characterized by means of photoluminescence measurements. The kinetics of luminescence were measured in order to analyze the energy transfer between ^{3}P$_0$ and ^{1}D$_2$ excited states that also take an active role in the persistent luminescence process. It was found that an increase in the crystallite size led to a higher energy transfer from the ^{3}P$_0$ to ^{1}D$_2$ level and a change in the emission color. As such, it was studied for potential application in ratiometric optical thermometry. The effect was also investigated in terms of persistent luminescence. It was also found that the sintering pressure causes changes in the crystallographic parameters of the powders and, in consequence, has a great impact on the optical properties of ceramics. The conducted research gives insights into the mechanism of persistent luminescence and expands the application field of optical storage materials.
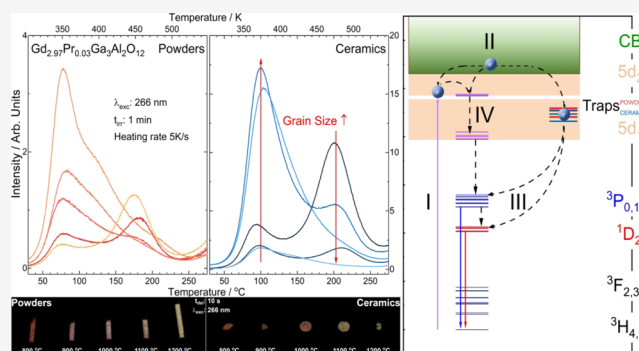
INTRODUCTION

Materials doped with praseodymium ions are very interesting due to the fact that it is possible to obtain structures that emit light in the red color range. The aforementioned emission color allows for various applications, such as in electronics, warning signs, LED displays, or medicine. Furthermore, the Pr ion is very often used as an admixture in various compound groups such as perovskites,[1] phosphates,[2,3] or garnets.[4,5] Even now, lots of new research are being carried out in this area, and as such recently a new concept for the improvement of orange-red emission based on the Pr^{3+}/Ce^{3+} combination has been presented.[6] From all of the aforementioned compound groups, garnets in particular have attracted the attention of researchers due to their chemical stability,[7] high quantum efficiency of rare-earth (RE)-doped structures,[8] and possibility of tuning optical properties by cationic substitution.[9] The most well-known and studied garnet structures are YAG,[10,11] LuAG,[12] and GGG.[13] However, there are several garnets with compositions, which are more complex, and, thanks to that often gain new unique properties. For example, Y$_3$Fe$_5$O$_{12}$ (YIG) is used in electronics,[14] Li$_7$La$_3$Zr$_2$O$_{12}$ (LLZ) in solid-state batteries,[15] Ca$_2$LnZr$_2$Ga$_3$O$_{12}$ in white LEDs,[16] or Y$_3$Al$_2$Ga$_3$O$_{12}$ for bioimaging.[17]

There is also a significant interest in using Pr^{3+}-doped and co-doped materials as persistent luminescence phosphors.[18,19] Persistent luminescence is a phenomenon that describes the continued emission of light from a phosphor even after the ceasing of irradiation for up to a couple of hours.[20] It is based on the slow release of electrons from traps that have accumulated there during the irradiation of the material. Most of such compounds exhibit a strong emission in the green region. However, due to the aforementioned different applications, it is desirable to obtain a material exhibiting a red color emission. For example, red warning signs are perceived by humans as more important, and biomaterials that emit red light can also penetrate through human tissues within the so-called biological windows.[21] Persistent luminescent phosphors also offer a remarkable advantage as optical storage materials where the phenomenon of capturing the electrons or holes in
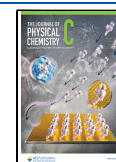
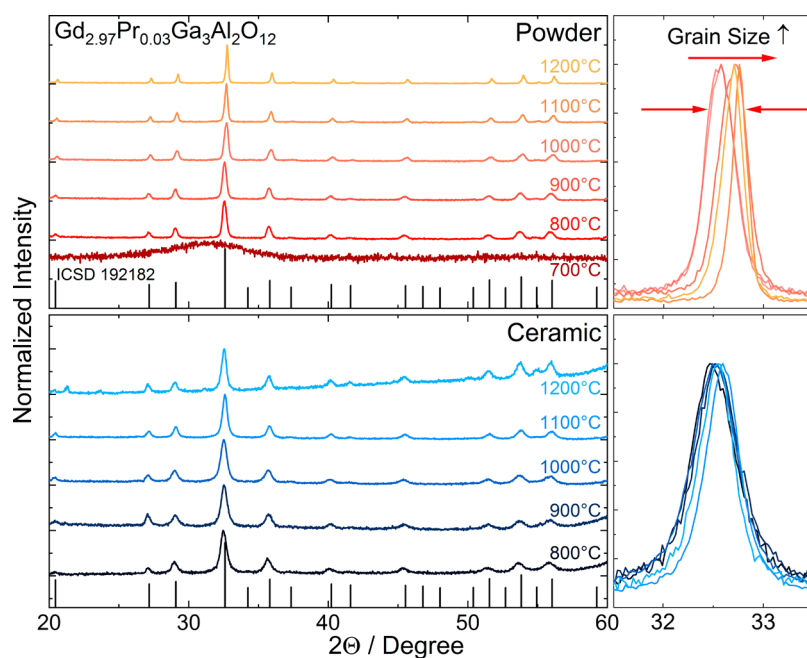**Figure 1.** XRD patterns of $Gd_{2.97}Pr_{0.03}Ga_3Al_2O_{12}$ powders calcined at different temperatures (top) and the ceramics sintered from them (bottom).

trap centers can be utilized.[22] The ultraviolet B (UVB) persistent luminescent materials are also used in the field of anti-counterfeiting and encryption applications.[23]

The aim of this work is to investigate the impact of the crystallite size on the persistent luminescence properties of $Gd_{2.97}Pr_{0.03}Ga_3Al_2O_{12}$. It has also been shown in our previous papers that in ceramics composed of nanosized particles, sintering pressure may affect the optical properties of the structures.[24] Therefore, a series of ceramics with grains from tens to hundreds of nanometers were prepared and investigated. All experiments were carried out in order to analyze the possibility of modulation of persistent luminescence color and duration. This was done because it is an essential factor on the aspect of future applications in temperature sensing, anti-counterfeiting, or optical information storage. It was found that by changing the crystallite size and applying pressure during ceramic sintering, it is possible to modulate persistent luminescence color and duration. Based on the obtained results, a mechanism of persistent luminescence was proposed and discussed.

■ EXPERIMENTAL SECTION

The powders used in the experiment were prepared using the sol−gel method based on a modified technique developed by Pechini.[25] The stoichiometric amounts of gadolinium (Gd_2O_3, 99.99% Sigma-Aldrich) and praseodymium oxide (Pr_6O_{11}, 99.99% Sigma-Aldrich) in a molar ratio of 99:1 were dissolved in concentrated nitric acid. The solution was then evaporated and recrystallized three times to remove excess nitric acid. Gallium and aluminum ions were added in the form of hydrated nitrates [$Ga(NO_3)_3 \cdot xH_2O$, 99.9% Sigma-Aldrich; $Al(NO_3)_3 \cdot 9H_2O$, 98+% Sigma-Aldrich]. Citric acid (anhydrous, 99.5+%, ACS) as a chelating agent and ethylene glycol (Reagent grade, POCH) as a polymer cross-linker were also added to the solution. The solutions were stirred for 3 h and then placed in a drying furnace at 90 °C for 7 days. As a result, a brown resin was obtained that was put into crucibles and calcined in air at various temperatures for 8 h. The obtained

product was ground into a fine powder in an agate mortar. The powder was then used in order to obtain ceramics. Ceramics were sintered using a low-temperature high-pressure method.[26] The powder was pressed at room temperature to a 5 mm diameter pellet. Then, the pellet (called green body) was placed in a $CaCO_3$ container with a special shape. A graphite heater was used for sintering ceramics inside the container by means of resistance heating. The applied pressure was equal to 8 GPa and the sintering temperature was maintained for 1 min. $Gd_3Ga_3Al_2O_{12}$ crystal nominally doped with 0.1 at. % of Pr^{3+} used in some experiments for comparison was grown by the Czochralski method under a nitrogen atmosphere on a ⟨111⟩ plane-oriented seed, with a pulling rate of 2.5 mm/h and a rotation speed of 20 rpm.

Equipment. X-ray powder diffraction patterns were collected by a X'PERT PRO PANalytical diffractometer using Cu K$\alpha_{1,2}$ radiation to evaluate the structure of the samples. Based on the XRD patterns, Rietveld analysis was applied to calculate the structural parameters of the samples using X'Pert pro analysis software. The morphology and microstructure of the powders were investigated using transmission electron microscopy (TEM) (Philips CM-20 SuperTwin operating at 160 kV). For calculations of the grain size distribution and average crystallite size, an ImageJ software was used.[27] The excitation and emission spectra were recorded using an FLS980 fluorescence spectrometer (Edinburgh Instruments) equipped with a holographic grating of 1800 lines per mm, blazed at 300 mm focal length monochromators in the Czerny Turner configuration, a 450 W xenon lamp as an excitation source, and a Hamamatsu R928P photomultiplier tube (PMT) as a detector. All spectra were corrected on a holographic grating resolution, xenon lamp emission spectra, and PMT sensitivity. Time-resolved luminescence spectra were acquired employing a grating spectrograph (Princeton Instr. Model Acton 2500i) coupled to a streak camera (Hamamatsu model C5680), which operates in the 200−1100 nm spectral region with a temporal resolution of 20 ps. As an excitation source, a femtosecond laser (Coherent Model "Libra") was

used, which delivers a train of 89 fs pulses. To obtain light pulses at the required wavelengths (285 and 445 nm), the laser was coupled to an optical parametric amplifier (Light Conversion Model "OPerA"). The luminescence kinetics was measured using short (4 ns) pulses delivered by an optical parametric oscillator OPO (Continuum, Surelite I) pumped by the third harmonic of a Nd:YAG laser. The luminescence was dispersed by a Zeiss 1 m double-grating monochromator GDM-1000 and detected by a Hamamatsu R-928 PMT. The decay signal was detected, averaged, and stored with a Tektronix MDO 4054B-3 oscilloscope. The persistent luminescence was measured using a SILVER-Nova Super Range TE Cooled Spectrometer (StallarNet Inc.) with a 100 μm slit and a 266 nm CNI laser diode (50 mW) as an excitation source. The persistent luminescence spectra were recorded 5 s after ceasing 1 min of irradiation. The thermoluminescence (TL) glow curves and fading times were detected by a Lexsyg Research fully automated TL/OSL reader from Freiberg Instruments GmbH for each sample at the same conditions. As an irradiation source, a 266 nm CNI laser diode (50 mW) was used. The TL glow curves were collected with a Hamamatsu R13456 PMT. The TL curves were recorded from 300 to 600 K at a heating rate 5 K/s after ceasing 1 min of irradiation with a 50 mW 266 nm laser diode. All numerical computations were done using the OriginLab Origin v2019b software. The XPS analyses were carried out with a Kratos Axis Supra spectrometer using a monochromatic Al K(alpha) source (25 mA, 15 kV). The instrument work function was calibrated to give a binding energy (BE) of 83.96 eV for the Au $4f_{7/2}$ line for metallic gold, and the spectrometer dispersion was adjusted to give a BE of 932.62 eV for the Cu $2p_{3/2}$ line of metallic copper. High-resolution analyses were carried out with an analysis area of 300 × 700 μm and a pass energy of 20 eV. Spectra have been charge-corrected to the main line of the carbon 1s spectrum (adventitious carbon) set to 284.8 eV. Spectra were analyzed using CasaXPS software (version 2.3.23rev1.1R).

RESULTS AND DISCUSSION

Structure Characterization. The XRD patterns measured for the $Gd_{2.97}Pr_{0.03}Ga_3Al_2O_{12}$ powders calcined at different temperatures and ceramics prepared from them (Figure 1) match well with the cubic structure of $Gd_3Ga_3Al_2O_{12}$ (ICSD 192182). It was shown that compounds start to crystallize above 700 °C. The characteristic peaks assigned to the GGAG structure were observed at and above 800 °C without any additional reflections arising from impurity phases. The powders crystallized in the cubic crystal structure with a $Ia\bar{3}d$ ($Z = 8$) space group, where Gd^{3+} ions enter dodecahedral positions surrounded by eight oxygen atoms (positions 24c in Wyckoff notation). Eight coordinated Gd^{3+} have ionic radii of 1.053 Å,[28] therefore doping with 1 mol % of Pr^{3+}, which has an ionic radii of 1.126 Å,[28] only slightly affect the structure of the matrix. It was observed that with the increase in the calcination temperature, diffraction peaks become narrower and move to higher 2θ angles (Figure 1 right). This suggests a shrinkage of the unit cell or introduction of stress into the lattice. Rietveld analysis showed that with the increasing calcination temperature, cell parameters as well as strains decreases (Table 1). Such behavior has been already observed by us in our previous work[29] and is related to the defects induced by the small size and high surface to volume ion ratio. After application of high pressure, it can be observed that a broadening of the reflections

Table 1. Structural Parameters of $Gd_{2.97}Pr_{0.03}Ga_3Al_2O_{12}$ Powders Calcined at Different Temperatures and Ceramics Sintered from Them

calc. temp. (°C)	size (nm)	a (Å)	strain (%)	bond length (Å)	
				Gd/Pr−O_T	Gd/Pr−O_O
Powders					
800	28	12.31(1)	0.036	2.424(9)	2.526(9)
900	29	12.29(6)	0.041	2.422(2)	2.524(2)
1000	31	12.28(6)	0.037	2.420(9)	2.522(8)
1100	43	12.27(4)	0.027	2.418(2)	2.520(0)
1200	74	12.27(0)	0.018	2.417(3)	2.519(1)
Ceramics					
800	16	12.33(6)	0.073	2.429(5)	2.531(7)
900	16	12.29(2)	0.067	2.421(0)	2.522(9)
1000	17	12.30(6)	0.072	2.422(0)	2.524(0)
1100	22	12.28(7)	0.054	2.420(4)	2.522(2)
1200	23	12.28(4)	0.051	2.419(7)	2.521(6)

occurs. This has been assigned to the introduction of stresses into the crystal lattice and the reduction of grain size associated with the decomposition of the layer on the grain surface (this effect is particularly noticeable for the smallest grains).[26] Similarly, to powder compounds in the XRD pattern of ceramics, a slight shift of the reflections toward higher angles was observed, but the shift was much weaker in this case. As mentioned before, Gd^{3+} and the substituting Pr^{3+} ions occupy dodecahedral positions, surrounded by eight oxygen atoms. The network of $Gd^{3+}/Pr^{3+}−O^{2-}$ and $O^{2-}−O^{2-}$ creates an edge of the dodecahedral site (with four octahedral and six tetrahedral sites), and the bond length between these ions has a great impact on the spectroscopic properties of Pr^{3+}.

For this reason, Rietveld refinement analysis was used to calculate the impact of the calcination temperature of the powder and sintering pressure on the bond length between Gd^{3+}/Pr^{3+} and O^{2-} occupying tetrahedral (O_T) and octahedral (O_O) sites (Table 1). It can be observed that a decrease in the bond length was determined with an increase in the calcination temperature of the powders. Interestingly, by applying pressure, the bond length also increases. It may be an effect of a tetragonal distortion observed in garnets, which is induced by high pressure acting on the unit cell. This has a great impact on the changes in spectroscopic properties of the ceramics.

TEM images were taken for all powders in order to confirm the crystallite size and check their morphology (Figure 2). It can be seen that with the increase of sintering temperature, the size of the crystallites also increases. For all calcination temperatures, the shape of the crystallites was smooth and rounded, forming oblong structures. With the increase of the calcination temperature, the crystallites sinter together and form larger grains and aggregates. The distribution of the grain size varied and for the highest calcination temperature, it was found that crystallites range in a size from 200 to 1000 nm. For the lowest temperature, the grain size distribution was narrower and the average crystallite size being about 13 nm.

Absorption, Excitation, Emission, and Luminescence Kinetics of $Gd_{2.97}Pr_{0.03}Ga_3Al_2O_{12}$. A direct consequence of the reduction in the lattice constant and the bond length should be an observable increase in the band gap energy.[30] It can be best observed for nanocrystals calcined at the lowest temperatures when the grain size was the smallest, but the lattice constant was the biggest. This is the result of surface to
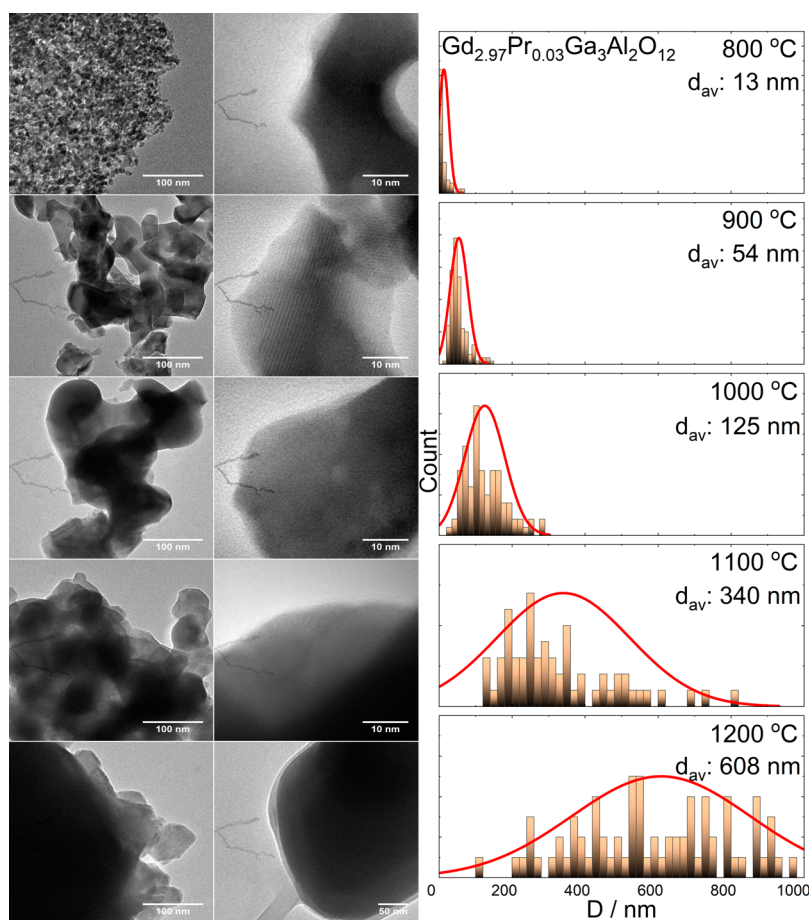
Figure 2. TEM images of $Gd_{2.97}Pr_{0.03}Ga_3Al_2O_{12}$ powders calcined at different temperatures and size distribution analysis.
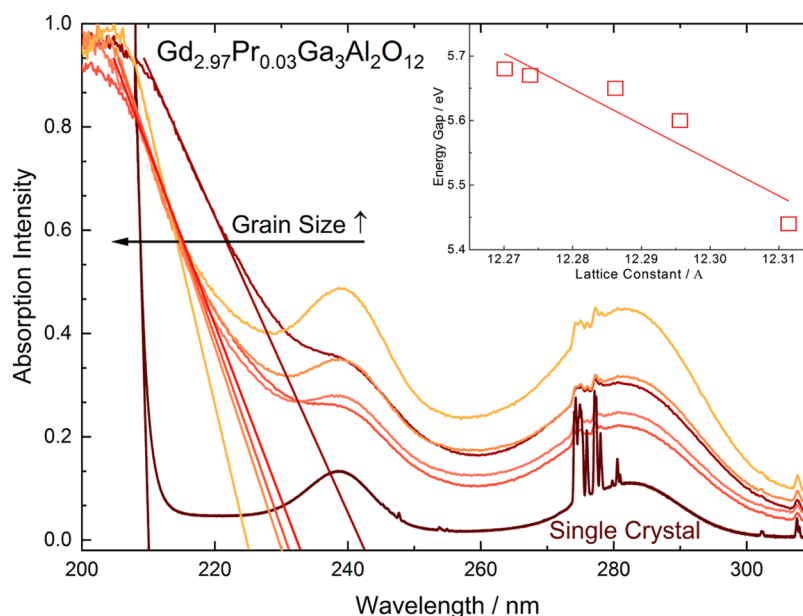

Figure 3. Diffuse reflectance spectra registered for $Gd_{2.97}Pr_{0.03}Ga_3Al_2O_{12}$ powders and single crystals.

volume ion ratio, where for the smallest grains, the cell units in the shell have a higher impact on the structural, and in consequence optical, properties, as compared to bigger grains. As the energy gap is inversely proportional to the interatomic distance, a shift should be observed for the energy band gap toward higher energies with the increase in grain sizes

(decrease of the bond length). To evaluate this assumption, absorption spectrum of the GGAG single crystal doped with 0.1 at. % Pr^{3+} was measured and compared with the diffuse reflectance spectra of the powders calcined at different temperatures (Figure 3). Because in powder compounds, the concentration of surface ions is higher than that for single
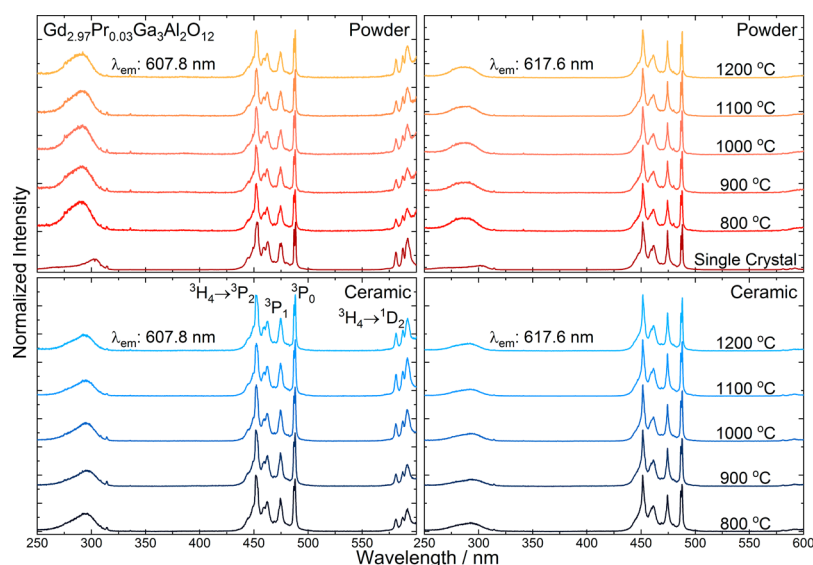
Figure 4. Excitation spectra of $Gd_{2.97}Pr_{0.03}Ga_3Al_2O_{12}$ powders and ceramics, recorded for emission from the $^1D_2$ (left) and $^3P_0$ (right) multiplets.

crystals and the incorporation of the luminescent ions affect the UV absorption edge of GGAG and may shift it between 209 and 230 nm (5.93−5.39 eV)[31,32] the spectra measured for single crystals is shown only for an error related to the nonlinearity of the mirrors used during the measurement. However, because the measuring system was the same for all powders, the changes observed in the position of the absorption edge can be regarded as being dependent on the grain size. For the determination of band gap energy (E_g), the following common formula was used[33]

$$(\alpha h \nu)^n = A(h\nu - E_g) \tag{1}$$

where $n = 2$ means direct band gap, $n = 1/2$ indirect one, α is the absorption coefficient, $h\nu$ is the energy, and A is a constant of material under study. From the spectra, absorption edge energy gap (E_g) value was calculated for all samples with $n = 2$. For GGAG single crystal doped with 0.1 at. % Pr^{3+}, the absorption edge is located at 209.3 nm (5.92 eV). For the powders calcined at 800, 900, 100, 1100, and 1200 °C, the energy gap is equal to 5.44, 5.60, 5.65, 5.67, and 5.68 eV, respectively (three significant numbers have been selected here due to the fact that the calculation error has three decimal place accuracy). This shows that the size of the grains as well as surface ions (that are responsible also for the unit cell expansion) have a great impact on the spectroscopic properties of $Gd_{2.97}Pr_{0.03}Ga_3Al_2O_{12}$. Because the ceramics were not transparent, the measurements for them were also made in the reflectance mode (Figure S1), but, in this case, at the lowest wavelengths (below 250 nm), the light scattering on their surface did not allow one to determine the absorption edge. Another interesting fact observed in reflectance spectra is that the allowed 4f−5d transition of Pr^{3+} with maximum at about 238 nm for the smallest grains overlaps with the absorption edge of the matrix. As such, this may have a significant impact on the persistent luminescence due to the higher probability of energy transfer via the conduction band.

The excitation spectra of powders calcined at different temperatures and ceramics prepared from them were registered at room temperature (Figure 4). The left side of this figure shows the excitation of the $^1D_2$ state (observed for the $^1D_2 \rightarrow$ $^3H_4$ transition at 607.8 nm), whereas the right side the

excitation of the $^3P_0$ multiplet (observed for the $^3P_0 \rightarrow$ $^3H_6$ transition, 617.6 nm). All excitation spectra ($^1D_2$ and $^3P_0$) were composed of sharp lines and were assigned to f−f transitions in Pr^{3+} ions, observed at 451, 462, 474, 488, and 591 nm corresponding to $^3P_2$, $^1L_6$, $^3P_1$, $^3P_0$, and $^1D_2$ levels, respectively. At lower wavelengths, characteristic peaks associated with Gd^{3+} ions are observed, corresponding with the intraconfigural transitions from the ground state $^8S_{7/2}$ to $^6P_{7/2}$ (308.5) and $^6P_{5/2}$ (314 nm) levels. This shows energy transfer from matrix component Gd^{3+} to optically active Pr^{3+}. The positions of all lines were confirmed with the absorption spectrum of GGAG single crystals doped with 0.1 at. % of Pr^{3+} (Figure 3).

In all spectra, a broad band with a maximum at around 288 and 295 nm was observed for both powders and ceramics, respectively. This band corresponds to $^4f_2 \rightarrow {}^4f_1{}^5d_1$ transition. It can be seen that the 5d band is much stronger for powders as compared to ceramics. This may suggest that in the case of ceramics part of the energy is transferred directly to the host matrix. It can also be observed that the intensity of the band is the highest for compounds with smaller particle sizes and with an increase in the grain size, the intensity of the 5d band decreases. For the single crystal, intensity of the bands was much lower and separation of the band into two components is clearly observed. The bands peaked at 285 and 240 nm and were assigned to the lowest $4f({}^3H_4) \rightarrow 5d_1$ and $4f({}^3H_4) \rightarrow 5d_2$ transitions, respectively.[34] It is worthy to note that when comparing to single crystals, in the case of both powders and ceramics, both 5d bands were closer together and shifted toward higher energy. The interfered areas of the f−d bands near 290 nm and the f−f $^3P_2$, $^1L_6$, $^3P_1$, and $^3P_0$ bands in blue (^3P_J) are gathered in Table 2.

Overall, emission spectra in the region of 470−750 nm are presented in Figure 5. The spectra are composed of transitions originating mainly in the $^3P_0$ and $^1D_2$ levels. The most intense line is situated at 486 nm and was assigned to the $^3P_0 \rightarrow {}^3H_4$ transition. The band in the region of 525−575 nm was assigned to the transitions from the $^3P_1$ and $^3P_0$ state to the $^3H_5$ level. The $^3P_0-{}^3H_5$ ($\Delta J = 5$) transition is forbidden due to selection rules in the frame of the Judd-Ofelt theory;[35−38] however, in opposition to other compounds[1,39,40] is easily observable in garnets. Additionally, due to Boltzmann

Table 2. Ratios of 5d to $^1D_2$ and $^3P_0$ Levels Observed for $Gd_{2.97}Pr_{0.03}Ga_3Al_2O_{12}$ Powders and Ceramics

calc. temp. (°C)	$^1D_2$ area			$^3P_0$ area		
	$^1D_2$	5d	ratio 5d/$^1D_2$	^3P_J	5d	ratio 5d/^3P_J
			Powder			
800	16.82	19.27	1.15	15.37	9.49	0.62
900	16.60	17.10	1.03	14.84	7.56	0.51
1000	16.06	18.40	1.15	13.90	8.14	0.59
1100	16.22	15.71	0.97	14.33	6.56	0.46
1200	16.64	15.06	0.91	14.79	7.10	0.48
			Ceramic			
800	18.33	9.21	0.50	15.61	4.99	0.32
900	18.29	7.93	0.43	15.54	4.07	0.26
1000	16.60	8.74	0.53	14.06	4.29	0.30
1100	17.31	7.55	0.44	15.64	3.70	0.24
1200	17.47	7.91	0.45	14.34	4.07	0.28

population levels at 300 K, an allowed ($\Delta J = 4$) transition from the $^3P_1$ excited state to the $^3H_5$ multiplet was seen at about 533 nm. Observant readers can find that the band at 607 nm (Figure 6) strongly depends on the calcination temperature. This band was ascribed to the $^1D_2 \rightarrow {}^3H_4$ transition. The transitions, in which the $\Delta J = 2$, are known as hypersensitive transitions and are maximally dependent on the environment near the lanthanide ions. It has been found that the strength of these transitions depends more on the electronegativity of the ligand than the symmetry.[41] However, in the case when all ligands are the same (e.g., oxygen atoms), it describes the symmetry. In the presented system, oxygen is the only type of the ligand and the change in the strength of $^1D_2 - {}^3H_4$ transition depends on the grain size, bond length, and the induced strain. In the case, when strain is lower and the size of the grains is larger the intensity of this band should be smaller. This fact is in full agreement with data presented in Table 1 and Figure 2. By increasing the temperature from 800 to 1200 °C, we can observe reduction in strain. It is interesting that after the application of pressure the intensity of this band increases as compared to the powders used for sintering. This behavior can be explained by continuing the discussions

outlined above. During sintering in the ceramics due to the large forces acting on the grains under a very high pressure, a large strain was induced in all cases. This strain has been "frozen" in the ceramics[24] and after the sintering process may act as an additional defect in the structure. Another important fact is that under the high pressure a part of the surface in small crystallites may decompose, which leads to a decrease of the grain size of ceramics. Furthermore, as it was shown above, the bond lengths in the ceramics also increases as compared to powders. Such processes in the ceramic lead to the change in the crystal environment of the Pr^{3+} and, in consequence, change to affect energy transfer between the 5d level and $^3P_0$ and $^1D_2$ multiplets.

Figure 7 shows luminescence spectra in the region of 475−675 nm recorded with femtosecond excitation with 285 and 445 nm wavelengths and streak camera collection. Such equipment allows us to observe the changes in the luminescence at different time-widows. For better clarity, the time windows after the initial pulse were: 0−200, 200−400, and 400−600 μs. The 6a and 6b spectra look rather similar except for the 600−650 μs fragment that has been discussed earlier. The dominant band was situated near 487 nm and was assigned to the $^3P_0 - {}^3H_4$ transition. In the next time window of 200−400 μs (6c) under 285 nm excitation luminescence, it was observed originating from both the $^3P_0$ and $^1D_2$ multiplets. In comparison to the 6a spectrum, the luminescence of the $^1D_2$ level, situated at ~607 nm, is much stronger and possessed the same intensity as the arising $^3P_0$ state. When the excitation wavelength is changed to 445 nm (6d), only the emission from the $^1D_2$ state is now seen. Next spectra (6e, f), for a time window of 400−600 μs, show that excitation into the $^3P_2$ (f−f transition) at 445 nm was finished with the emission from $^1D_2$ multiplet, whereas upon 285 nm excitation (f−d excitation band) luminescence coming both the $^3P_0$ and $^1D_2$ states was seen.

Kinetics of Luminescence. The lifetime of the $^3P_0$ state should differ as compared to the $^1D_2$ multiplet as was shown in earlier works.[42] The lifetime values for the $^3P_0$ and $^1D_2$ states have been calculated to be 21 and 206 μs, respectively. Figure S2 shows the decay curves of luminescence recorded for $^3P_0$
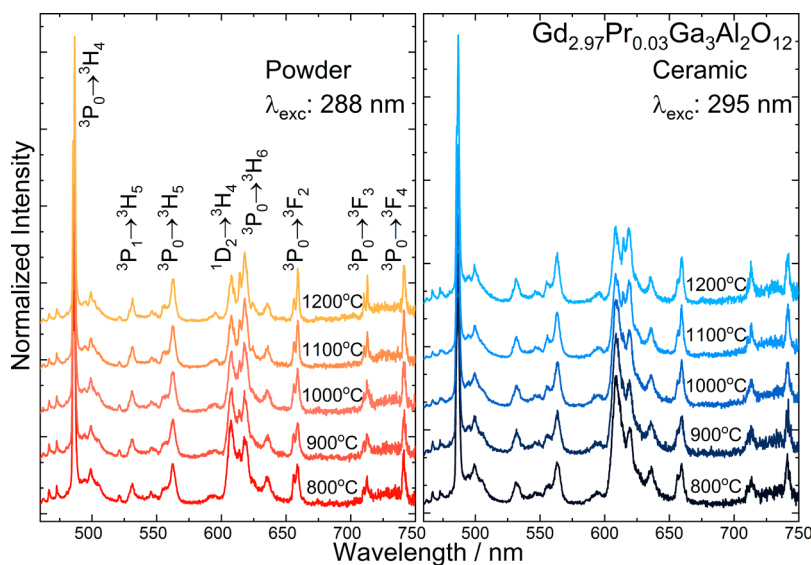
Figure 5. Emission spectra of $Gd_{2.97}Pr_{0.03}Ga_3Al_2O_{12}$ powders (left) and ceramics (right).
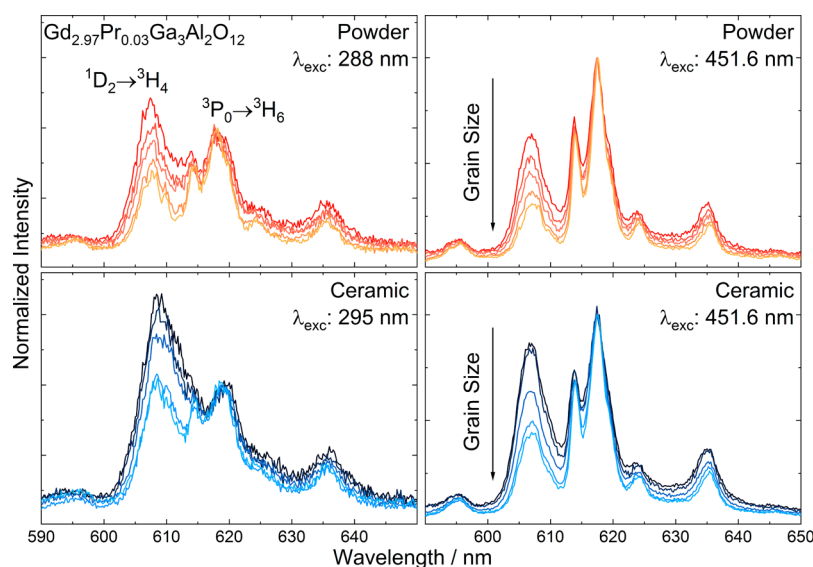
Figure 6. $^1D_2 \rightarrow {}^3H_4$ and $^3P_0 \rightarrow {}^3H_6$ transitions measured for $Gd_{2.97}Pr_{0.03}Ga_3Al_2O_{12}$ powders (top) and ceramics (bottom) under UV (left) and vis (right) excitation.

(487 and 565 nm) and $^1D_2$ (607 nm) states under 285 and 445 nm excitation recorded at 200 or 1000 μs time windows. As one can see, the decay profiles for excitation under 445 nm were much faster than for 285 nm. Probably, the excitation with 285 nm not only excite Pr^{3+} into the 4f–5d band but also the energy is stored up in some defects and is released from them slowly. It can be especially seen from the curve observed at 487 nm. Detailed information about the behavior of decay curves of the $^3P_0$ and $^1D_2$ luminescent states is presented in Figure 8 and Table 3. In this case, the metastable multiplets were excited directly with the use of an optical parametric oscillator (OPO). One can see that these curves in the case when grains were the smallest were non-exponential. Therefore, for comparison the average lifetime has been used,[43] which is defined as

$$\tau_m = \frac{\int t I \, dt}{\int I \, dt} \qquad (2)$$

where where I is the intensity of luminescence and t represents time. For all analyzed calcination temperatures, the mean lifetimes do not differ much and are calculated to be 213 μs for the $^1D_2$ and 22 μs for the $^3P_0$ multiplets (see Table 3). These values are in agreement with the data published earlier as well as calculated in the frame of Kornienko Modification of the Judd–Ofelt Method.[42]

Temperature Sensitivity of $Gd_{2.97}Pr_{0.03}Ga_3Al_2O_{12}$. The emission spectra of $Gd_{2.97}Pr_{0.03}Ga_3Al_2O_{12}$ powders calcined at various temperatures as well as ceramics made from them were measured at the wide temperature range from 83 to 573 K (Figure S3). For better comparison, the spectra measured for both powders and ceramics made of the smallest grains are given in Figure 9. It can be noticed that the grain size and sintering pressure have a great impact on the energy transfer between f levels of Pr^{3+}. From the data given in the figure, it is clear that temperature dependencies are related the change in the grain size (annealing temperature) and the pressure applied in the sintering process. It should also be noted that for larger grains (annealed at a higher temperature), low-temperature spectra show a sharp peak at around 692 nm and a wide band between 750 and 850 nm. It may be caused by the

unintentional Cr^{3+} admixture appearance in the structure which is an impurity from the Al precursor used for the synthesis. As the infrared emission has been observed in the GGAG structure even at extremely low concentrations of Cr^{3+} (15 ppm),[44] the luminescence observed at low temperatures was assigned to the Cr^{3+} impurities from the precursor.

In order to check how the temperature influences the emission bands arising from individual levels, the integrated intensity at a given temperature was calculated for the four transitions (Figure 10). For the calculations $^3P_0 \rightarrow {}^3H_4$ (centroid at 492 nm), $^3P_1 \rightarrow {}^3H_5$ (at 540 nm), $^1D_2 \rightarrow {}^3H_4$ (at 603 nm), and $^3P_0 \rightarrow {}^3F_3$ (at 660 nm) transitions were used. Because part of the emission from $^1D_2$ to the ground state overlapped emission from the $^3P_0$ to $^3H_4$ level the calculations performed for this transition have the greatest error. For the samples composed of the smallest grains a decrease of the intensity of transitions from the $^3P_0$ excited state can be noticed with the rising temperature. While the intensity of transitions from $^1D_2$ and $^3P_1$ levels increases. For samples composed of larger grains, the situation changes and up to a certain temperature the intensity of all transitions increases with the temperature. It is interesting that the temperature when the intensity of particular transitions starts to decrease increases in the case when grains are bigger. Also, the point where the decrease in the intensity of the $^3P_0$ level transition intersects with the increase in the intensity of the $^1D_2$ transition shifts toward higher temperatures as the grain size increases. This phenomenon has been reported to be related to the ratio of the surface to volume ion ratio and participation of the "superficial" ions in electron–phonon interactions.[45] Recently, Bolek et al.[46] have shown that by engineering the band gap by varying the ratio of Ga to Al in garnets, it is possible to control the thermometric properties of these materials. In that work, similar modifications have been induced by changing the grain size. The observed phenomena also have a great impact on energy transfer between d and f excited levels, which leads to changes in the persistent luminescent properties.

The effect of the changes of the emission intensity as a function of temperature is commonly used for temperature
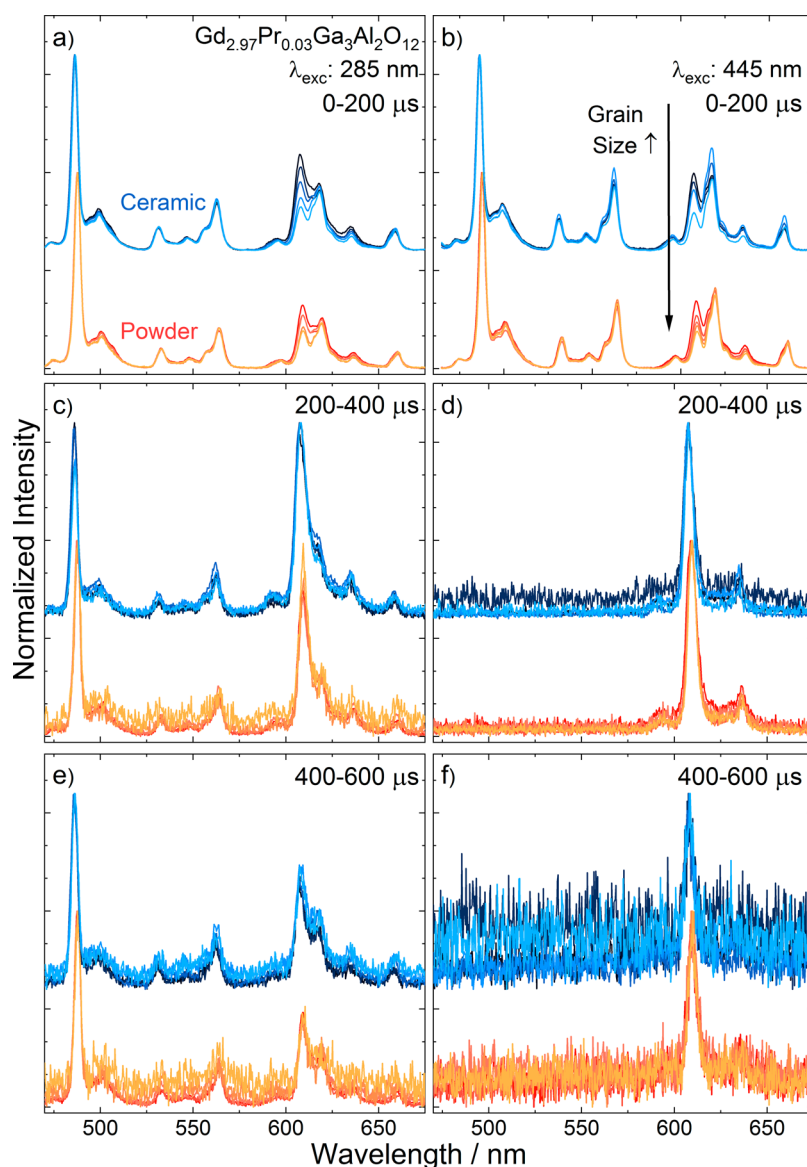
Figure 7. Time-resolved luminescence spectra of $^1D_2$ and $^3P_0$ multiplets of Pr^{3+} upon excitation at 285 and 445 nm measured for powders and ceramics.

sensing. In $Gd_{2.97}Pr_{0.03}Ga_3Al_2O_{12}$, several transitions can be used to calculate temperature dependencies, but from the application point of view, it is the most important to find the transition with the highest sensitivity as well as with the widest temperature range where this dependance is linear. The sensitivity based on the luminescence intensity ratio, S_r, can be expressed as

$$S_r = \frac{1}{LIR}\left|\frac{dLIR}{dT}\right| \times 100\% \tag{3}$$

where LIR is the luminescence intensity ratio of particular transitions.[45]

The LIR for all combinations of transitions in Pr^{3+} have been calculated and the integral intensity ratio between $^3P_0 \rightarrow {}^3H_5$ and $^1D_2 \rightarrow {}^3H_4$ transitions has been chosen as an optimal thermal sensor due to the unique value of LIR in the whole temperature range as well as the largest range of LIR values (Figure 11). It is caused by very low intensity dependence of the $^3P_0 \rightarrow {}^3H_5$ transition on temperature. The values of LIRs

were similar for powders and ceramics, and it has been found that these values are higher for when compounds are made up of smaller grains. The LIR values change from about 0.5 for 83 K up to about 2.0–2.5 for 573 K.

The relative sensitivity according to formula (3) has been calculated for ceramic as well as for powder samples. It was found that the grain size effect is observed and the relative sensitivity increase with the grain size. The relative temperature sensitivity is the highest for the powder with the biggest grains (highest calcination temperature) and ceramic prepared from them and have values of 0.423 and 0.380%/K, respectively (Table 4). For the lowest annealing temperature, deviations from the dependence of the grain size on the temperature sensitivity can be observed, which may be the effect of a much larger share of surface ions in the temperature effect. Higher temperature sensitivity may lead to the faster electron transfer from the traps to the conduction band and in consequence improving the persistent luminescence. However, it is also important to mention that this effect takes place mainly on the surface of the crystallites, therefore in ceramics,
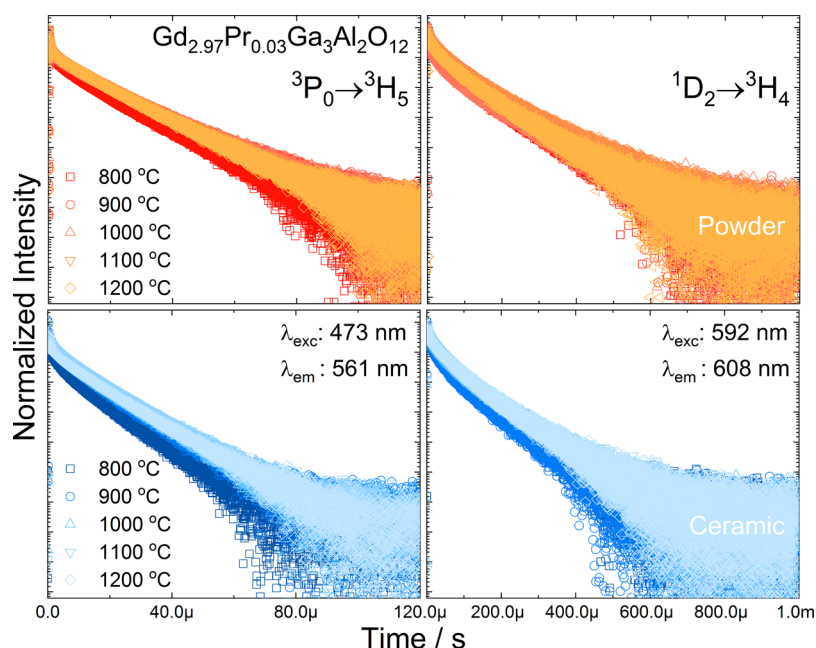
Figure 8. Luminescence decay curves registered for $^3P_0$ (left) and $^1D_2$ (right) multiplets for the $Gd_{2.97}Pr_{0.03}Ga_3Al_2O_{12}$ powders (top) and ceramics (bottom).

Table 3. Measured Lifetimes and Efficiencies of $^1D_2$ and $^3P_0$ Multiplets in the $Gd_{2.97}Pr_{0.03}Ga_3Al_2O_{12}$ Powder and Ceramic Samples as the Function of Calcination Temperature

calc. temp. °C	lifetime µs		efficiency (η) %	
	$^1D_2$	$^3P_0$	$^1D_2$	$^3P_0$
	Powder			
800	200.51	20.36	90.14	88.10
900	217.45	22.85	97.75	98.87
1000	213.55	23.11	96.00	100.00
1100	222.44	22.53	100.00	97.50
1200	210.08	21.24	94.44	91.92
	Ceramic			
800	89.40	20.73	87.64	83.66
900	94.206	21.64	92.35	87.33
1000	97.93	22.63	96.00	91.32
1100	102.01	24.77	100.00	99.96
1200	97.67	24.78	95.75	100.00

where the "active" area is much smaller, this effect will be weaker.

Persistent Luminescence Spectra of $Gd_{2.97}Pr_{0.03}Ga_3Al_2O_{12}$. For $Gd_{2.97}Pr_{0.03}Ga_3Al_2O_{12}$ powders and ceramics, persistent luminescence spectra were measured after ceasing UV (266 nm) irradiation. It was found that after excitation with 450 nm (2.72 eV) light there was no persistent luminescence, which may indicate that this energy is too low to transfer carriers to the traps near the conduction band. Interestingly, despite high-energy excitation (266 nm, 4.66 eV), persistent luminescence from the 5d level was not observed as described by Yuan et al.[47] This is probably due to the overlapping of the 5d band with the absorption edge of the matrix and an immediate energy transfer to the lower energy levels. The samples were irradiated for 5 min and 10 s after switching off the excitation source, the emission spectra were collected (Figure 12). The persistent luminescence spectra are similar to the conventional luminescence indicating the same emitters (Pr^{3+}). The peaks in persistent luminescence spectra are broader as compared to the conventional luminescence because of the lower resolution of CCD camera used for measurements. Feng et al. has shown that for $Lu_3Ga_3Al_2O_{12}$ doped with a 0.3 mol % Pr^{3+} band corresponding to the $^1D_2 \rightarrow {}^3H_5$ transition is more intense in persistence than in conventional luminescence.[48] In the presented material, this effect is not observed due to higher concentrations of Pr^{3+} ions. This suggests that a part of the electrons released from the traps may pump to the $^1D_2$ level by direct energy transfer. The red component of the spectra associated with the emission from the $^1D_2$ level has the highest share in the total emission for powders obtained at the lowest temperatures (and ceramics obtained from them), for these samples the emission color is red. In the case of powders and ceramics with largest grains, the emission from this level is less intense, and the luminescence color is white/green. The calculations of the XY coordinates for powders and ceramics show that for ceramics the emission color has more red component as compared to the powders (Figure S4).

The luminescence fading curves were registered for all structures after ceasing 266 nm irradiation (Figure 13). The curves are presented in a logarithmic scale and it can be seen that they are multi exponential. All curves were fitted using the biexponential decay model, which indicates that the persistence luminescence process comprises of at least two different energy transfer processes. The fast component is related to bright emission coming from shallow traps and the longer component comes from deeper traps and is responsible for the longer duration of the emission. As shown in Figure 13, persistent luminescence was stronger and longer for the ceramic samples. This suggests that for ceramic sample trap depth is more broadly distributed and the deep ones have a greater contribution in the persistent luminescence. The calculation of the luminescence fading times shows that both components are longer for ceramic samples (Table 5). For
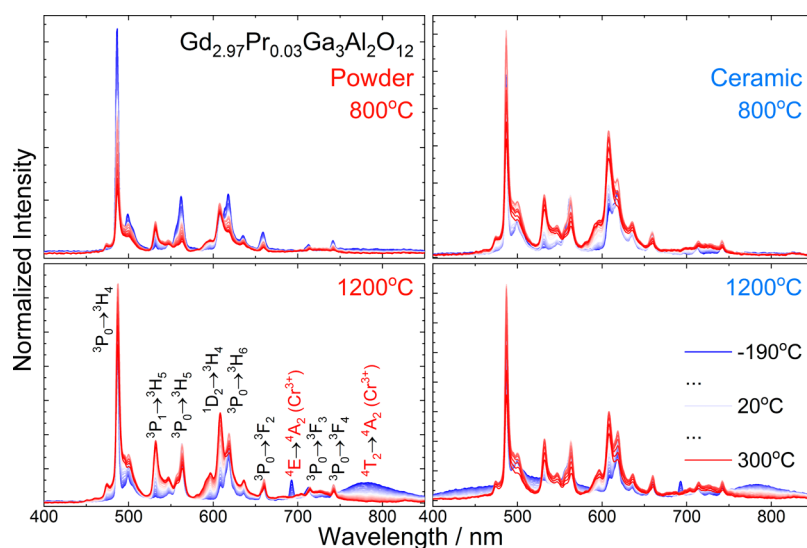
Figure 9. Luminescence spectra of $Gd_{2.97}Pr_{0.03}Ga_3Al_2O_{12}$ powder (left) and ceramics (right) with the smallest (top) and largest (bottom) grains registered in the temperature from 83 to 573 K.
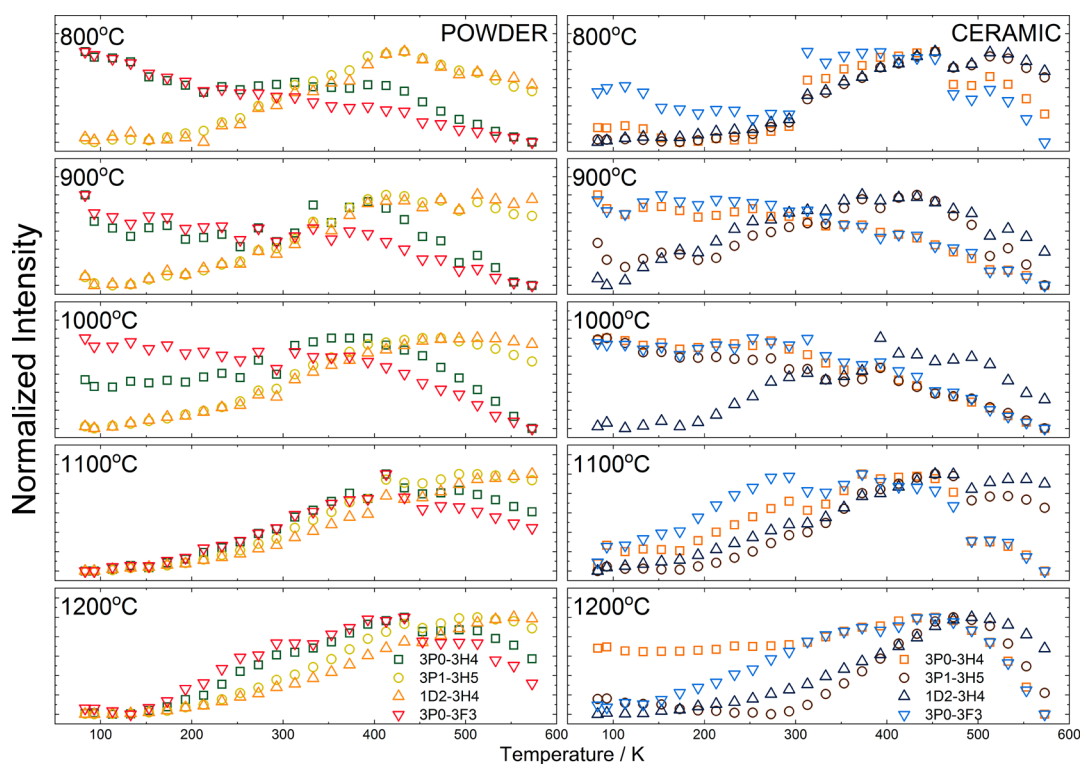

Figure 10. Changes in the emission intensity of individual transitions in the function of the temperature calculated for $Gd_{2.97}Pr_{0.03}Ga_3Al_2O_{12}$ powders (left) and ceramics (right).

slower component, the changes are less pronounced than for longer components, but it is clear that the sintering of the powders has a great impact on the distribution of trap depth.

Thermoluminescence $Gd_{2.97}Pr_{0.03}Ga_3Al_2O_{12}$. To investigate the release processes of stored energy from $Gd_{2.97}Pr_{0.03}Ga_3Al_2O_{12}$, TL curves were measured after irradiation with a UV laser diode (266 nm) over 300−600 K (Figure 14) temperature range. TL curves were measured for powder and ceramics 1 min after ceasing irradiation. For all structures, the glow curves were composed of at least three broad bands, and their intensity changes as a function of the grain size. It is interesting that for the smallest grains the most

intense band is located at higher temperatures (higher energy) and with an increase of crystallite size, the high energy band disappears and the intensity of the band observed at lower temperatures (lower energy) increases. This behavior is observed for both powders and ceramics. It may be related to the optical quality of crystallites that grow above certain temperatures and the relaxation processes which occur faster, with less electrons that can be trapped. It can be also observed that for the ceramics the bands are shifted toward higher temperatures (Table 5). This may explain longer emission from ceramic samples, as the energy needed to release the electrons from traps is higher and takes more time. Also, the
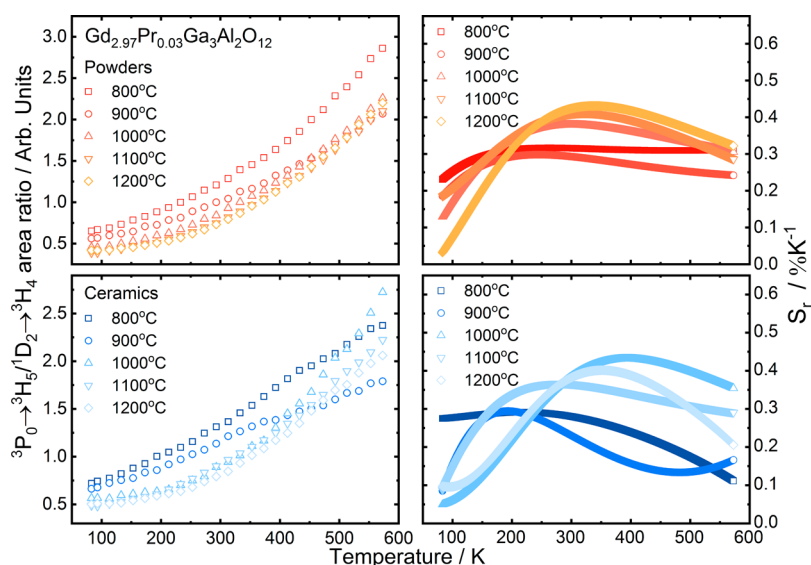
Figure 11. Luminescence intensity ratio (LIR) of $^3P_0 \rightarrow {}^3H_5$ and $^1D_2 \rightarrow {}^3H_4$ transitions of Pr^{3+} calculated for the powder and ceramic samples (left) and the relative sensitivity—S_r (right).

Table 4. Relative Temperature Sensitivity at 300 K Calculated for the $Gd_{2.97}Pr_{0.03}Ga_3Al_2O_{12}$ Powder and Ceramic Samples

calcination temperature (°C)	relative sensitivity @300 K (%/K)	
	powders	ceramics
800	0.315	0.280
900	0.293	0.231
1000	0.378	0.383
1100	0.408	0.365
1200	0.423	0.380

intensity of the low energy band was 5 times higher, which suggests that the same amount of energy released more

electrons, and therefore a more intensive emission is observed from ceramic samples. The change in the ratio of high to low temperature band has been also observed earlier by us in the case of Tb^{3+}-doped garnet and was related to the concentration of the dopant ion.[49] In this case, the concentration of the luminescent ion is constant and only the size of the grains is changing. This leads to the conclusion that in the case of persistent luminescence, energy transfer may take an active role in the surface ions, where the crystal field affecting optically active ions changes the most.

The glow curves were analyzed using the OriginLab 2019b software. The results of the fitting are presented in Table 6.

A simple analysis model was used based on the estimation of the trap depths from the location of the glow peak that has
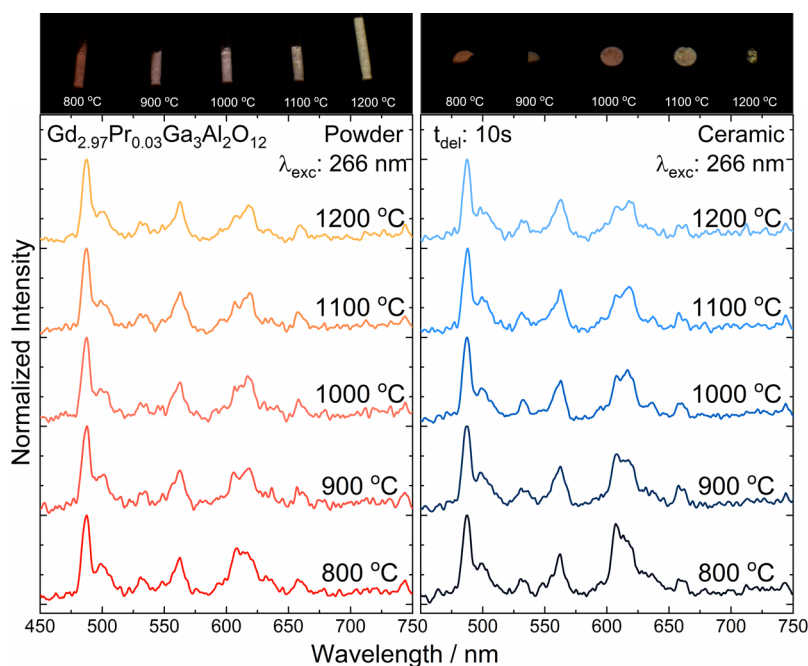

Figure 12. Persistent luminescence spectra of $Gd_{2.97}Pr_{0.03}Ga_3Al_2O_{12}$ powders and ceramics and the corresponding photos.
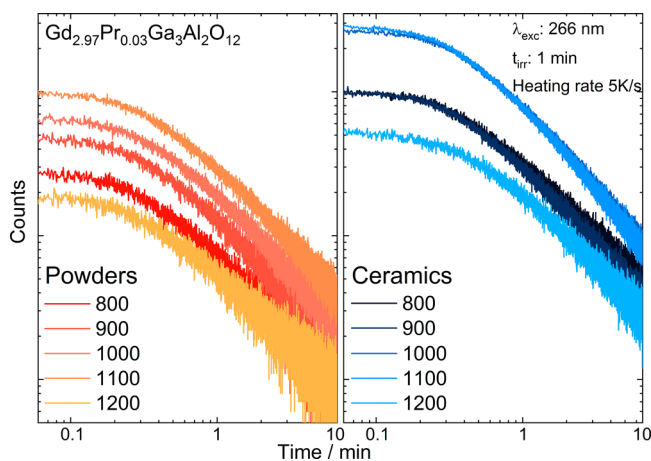
Figure 13. Fading of persistent luminescence registered for $Gd_{2.97}Pr_{0.03}Ga_3Al_2O_{12}$ powders and ceramics.

Table 5. Fading Time of Persistent Luminescence of $Gd_{2.97}Pr_{0.03}Ga_3Al_2O_{12}$ Powders and Ceramics

	fading time			
	powder		ceramic	
calc. temp. (°C)	τ_1 (s)	τ_2 (s)	τ_1 (s)	τ_2 (s)
800	35	164	39	183
900	36	162	38	172
1000	37	170	40	180
1100	37	173	38	172
1200	34	159	50	218

been proposed by Urbach.[50] This model introduces large simplifications and assumes that charge carriers recombine with luminescent centers and are not caught again by another trap, but it is used here to show the variation in depth and distribution of traps depending on the grain size of the powders and the applied pressure. The analysis shows several facts. First, it can be seen that for the powder energy of all traps is lower and after applying pressure, they become deeper. Second, the decrease of the contribution of deep traps with the

increase in the grain size was also noticed for both, powders and ceramics. Third, traps with the medium energy have similar contributions in all structures and in the case, when samples are made up of larger grains more shallow traps are observed. Lastly, traps with an average value of energy are likely to play the role of a bridge between deep and shallow traps and in view of this, despite the significant overall contribution to the distribution, they are inconspicuous in terms of changes in optical properties.

When considering the nature of the traps, two main facts should be taken into account. First is the use of the multivalent oxide Pr_6O_{11} as a precursor. During synthesis, the praseodymium ions may not be completely reduced and coexist in the matrix in a mixed-valence state (Pr^{3+}, Pr^{4+}). Second is the presence of the oxygen vacancies $V_o^{\bullet\bullet}$, resulting from calcination in an air atmosphere.

X-ray Photoelectron Spectroscopy of $Gd_{2.97}Pr_{0.03}Ga_3Al_2O_{12}$ Powders and Ceramics. To check for the presence of Pr^{4+} ions and to confirm the valence of praseodymium ions in the host, the X-ray photoelectron spectroscopy (XPS) analysis was performed (Figure 15). As a reference for Pr^{3+} and Pr^{3+}/Pr^{4+}, fitting models $PrNO_3 \cdot 6H_2O$ and Pr_6O_{11} compounds were used. Spectra obtained for both powders and ceramics demonstrate spin−orbit splitting ($3d_{3/2}$ and $3d_{5/2}$) and also multiplet splitting of Pr3d core level. The bands at 930.6, 935.5, 939.4, 947.6, 951.2, 956.0, and 960.0 eV are associated with the characteristic, complex chemical state of Pr^{4+}, and the ones at 928.9, 933.3, 949.5, 953.8, and 958.0 eV correspond to the Pr^{3+} state.[47,51,52] It can be noticed that the multiplet intensity decreases with the increase of the calcination temperature. This behavior is most probably related to the small concentration of Pr^{3+} ions and the size of the particles. It was shown by Baer[53] that the XPS penetration depth is dependent on the energy of the photoelectron and material, but nominally is considered to be about 10 nm. As such, for small particles, XPS senses the whole particle (the analyzer "sees" the signal from all present Pr^{3+} ions and not only from the surface); therefore, the signal may be strengthened. Unfortunately, this phenomenon is less visible in the case of powders and ceramics, as the scattering
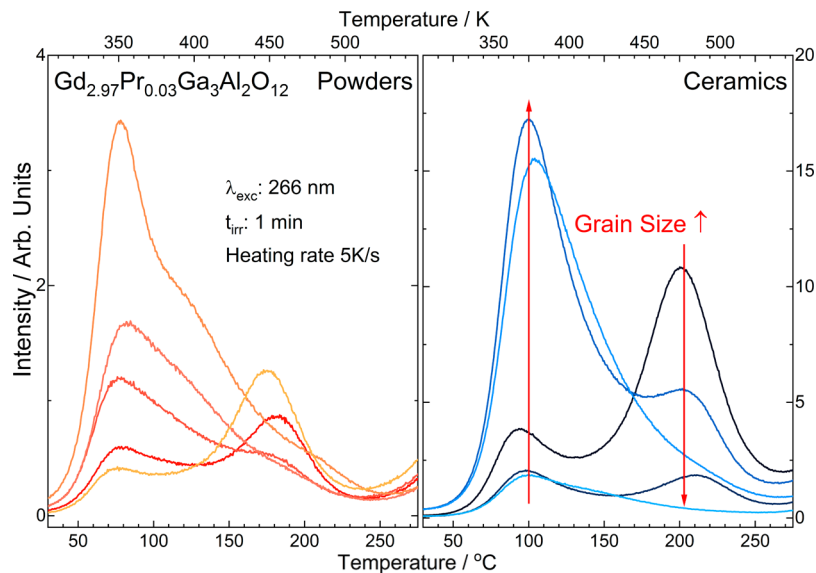

Figure 14. Thermoluminescence glow curves registered for $Gd_{2.97}Pr_{0.03}Ga_3Al_2O_{12}$ powders and ceramics.

Table 6. TL Glow Curve Parameters Calculated for $Gd_{2.97}Pr_{0.03}Ga_3Al_2O_{12}$ Powders and Ceramics

calc. temp. (°C)	TL parameters	powder			ceramic		
800	T/K	373	412	478	390	487	498
	E/eV	0.75	0.82	0.96	0.78	0.97	0.99
	share/%	17.5	30.0	52.5	7.6	63.4	28.9
900	T/K	369	397	461	392	428	506
	E/eV	0.74	0.79	0.92	0.78	0.86	1.01
	share/%	21.8	40.3	37.9	26.3	23.4	50.4
1000	T/K	373	402	447	393	419	494
	E/eV	0.75	0.80	0.89	0.79	0.84	0.99
	share/%	23.3	39.6	37.1	31.3	39.7	29.0
1100	T/K	373	401	455	395	420	464
	E/eV	0.75	0.80	0.91	0.79	0.84	0.93
	share/%	25.1	42.1	32.8	29.2	40.6	30.2
1200	T/K	371	408	472	393	423	479
	E/eV	0.74	0.82	0.94	0.79	0.85	0.96
	share/%	9.0	14.6	76.4	22.6	47.9	29.5
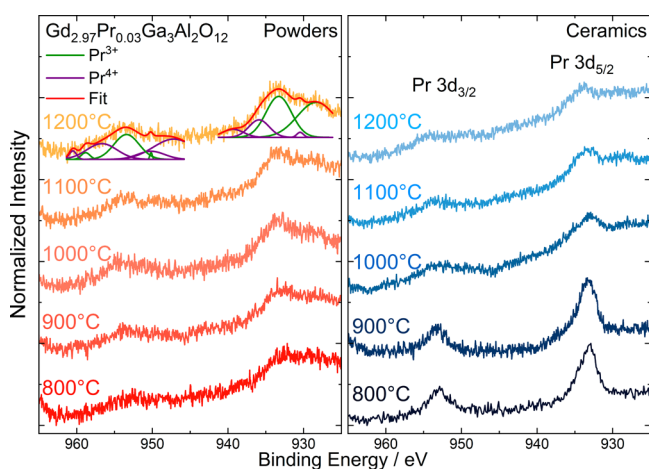
Figure 15. Pr 3d high-resolution XPS spectra of $Gd_{2.97}Pr_{0.03}Ga_3Al_2O_{12}$ powders and ceramics.

Table 7. Area Percentages of Pr^{3+}/Pr^{4+} Photoelectron Lines of $Gd_{2.97}Pr_{0.03}Ga_3Al_2O_{12}$ Powders and Ceramics

	area percentage of Pr^{3+} and Pr^{4+} ($3d_{3/2}$ and $3d_{5/2}$)	
T (°C)	Pr^{3+} (%)	Pr^{4+} (%)
	Powders	
800	83	17
900	81	19
1000	79	21
1100	84	16
1200	84	16
	Ceramics	
800	85	15
900	71	29
1000	82	18
1100	84	16
1200	84	16

there is much higher and the signal is much noisier. Analysis of the XPS spectra confirms the coexistence of Pr^{3+} and Pr^{4+} in powders and ceramics. For all samples, the Pr^{3+}/Pr^{4+} remains constant, only for the samples consisting of the smallest grains (900 and 1000 °C powders and ceramics 800, 900 and 1000 °C) a small deviation from the norm can be observed (Table 7). Considering that XPS is a surface-sensitive analysis method, this deviation may be a result of the fact that the surface/volume ion ratio for these samples is the biggest. It may be also the effect of hydroxyl group formation near the crystallite surface and the hygroscopic nature of praseodymium.[54] The Pr^{4+} in an 8 coordinated environment has an ionic radius of 0.96 Å,[28] which suggests that it will occupy the dodecahedral sites of Gd^{3+} ($r = 1.053$ Å at CN = 8) in $Gd_{2.97}Pr_{0.03}Ga_3Al_2O_{12}$. Therefore, it can be assumed that Pr^{4+} incorporated into the crystal lattice will generate a positive charge defect $Pr_{Gd}^{\bullet}$. Taking into account TL and XPS analyses, it can be assumed that the main role in the persistent luminescence will played by two types of positive charge defects. The Pr^{4+} incorporated into the crystal lattice will create $Pr_{Gd}^{\bullet}$ and calcination and sintering under an air atmosphere will introduce oxygen vacancies $V_o^{\bullet\bullet}$.

Mechanism of Persistent Luminescence. Based on the absorption data, the energy of band gap (the bottom of the CB was designated based on the calculations from the diffuse reflectance spectra and the energy of the valence band was estimated based on the Dorenbos's considerations regarding the location of divalent and trivalent lanthanide impurity levels[55] and two 5d levels were taken and together with exited levels registered in excitation spectra and trap depths calculated from thermoluminescence measurements a mechanism of persistent luminescence is proposed (Figure 16). Upon 266 nm irradiation, the electrons are excited from the ground state to the 5d level and due to relative small thermal activation energy also to the conduction band (I). Part of the electrons recombine directly with the excited states of Pr^{3+} and conventional luminescence is observed. Another part of the electrons is transferred through the conduction band to the traps located just below it where they are captured (II). Under continuous irradiation, the shallow and deeper traps are filled. After ceasing the irradiation under thermal stimulation at room temperature, the same route is used to transfer released electrons from shallow traps to the 5d and consequently, 4f levels ($^3P_{0,1,2}$ and $^1D_2$) of Pr^{3+}. The electrons from excited Pr^{3+} levels return to their ground state causing persistent luminescence (III). Simultaneously, the electrons captured in deeper traps may be transferred to the nearby ionized Pr^{3+} through direct tunneling, which also leads to the persistent luminescence. It is important to note that the energy of the traps in ceramics is higher (which means they lie further from the bottom of the conduction band but closer to the excited
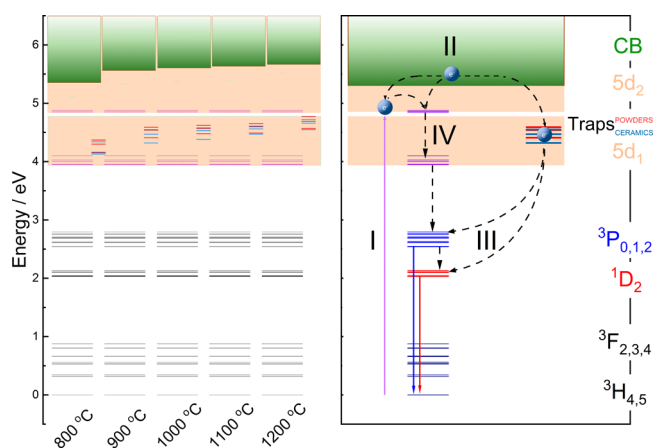
Figure 16. Mechanism of persistent luminescence in the $Gd_{2.97}Pr_{0.03}Ga_3Al_2O_{12}$ powders with different grain sizes and ceramics made of them.

levels of Pr^{3+}), which may promote direct energy transfer from the trap to the excited level of Pr^{3+} (IV). Because the share of deep traps in the samples made up out of the smallest crystallites (and after applying the pressure) is the highest, the probability of direct transfer to the $^1D_2$ level is greatest, which is seen as an increase in the share of red color in conventional and persistent luminescence for these materials.

CONCLUSIONS

A series of novel persistent luminescent powder and ceramic phosphors doped with praseodymium ions were successfully synthesized via a sol−gel method. For powders and ceramics composed of different size grains, a systematic study of their crystal structure indicated a well-crystalized cubic structure. A decrease in the $Pr^{3+}-O^{2-}$ bond length with an increase in the grain size for powders and ceramics was observed. In the case of ceramics, this is an effect of a tetragonal distortion observed in garnets induced by high pressure acting on the unit cell. This effect has a direct impact on the energy gap value. For the powders calcined from 800 to 1200 °C, the band gap energy is increased from 5.44 to 5.68 eV, respectively. It was found that the $^4f_2 \rightarrow {}^4f_1{}^5d_1$ transition is much stronger for the powder then for ceramics, which may suggest better energy transfer directly to the conduction band. It was also shown that the emission from the $^1D_2$ level strongly depends on the grain size. The change in the luminescence intensity observed for particular transitions as a function of the grain size was utilized for the temperature sensing and was linked to the release of electrons from traps in term of enhancement of persistent luminescence. The materials made up out of the biggest grains can be effectively activated by UV radiation and exhibit intense persistent luminescence in the visible range. The persistent luminescence mechanism was constructed based on the band gap energy calculated from absorption spectra, 4f and 5d levels extracted from emission and excitation spectra, type of the traps revealed from XPS measurements, and trap depths calculated from thermoluminescence measurements. The proposed model shows the effect of crystallite size and pressure applied during ceramic sintering on the efficiency of energy transfer and can be applied for the development of other compounds doped with Pr^{3+} exhibiting persistent luminescence.

ASSOCIATED CONTENT

⬢Ⓢ Supporting Information

The Supporting Information is available free of charge at https://pubs.acs.org/doi/10.1021/acs.jpcc.2c00672.

Results of diffuse reflectance of powders and ceramics, time resolved decay curves, luminescence spectra of all powders and ceramics measured from 83 to 573 K, and the CIE diagram (PDF)

AUTHOR INFORMATION

Corresponding Author

  Paweł Głuchowski − *Institute of Low Temperature and Structural Research PAS, PL-50422 Wroclaw, Poland;* ⓞ orcid.org/0000-0003-2566-1422; Email: p.gluchowski@intibs.pl

Authors

  Robert Tomala − *Institute of Low Temperature and Structural Research PAS, PL-50422 Wroclaw, Poland;* ⓞ orcid.org/0000-0003-2206-3080

  Daniela Kujawa − *Institute of Low Temperature and Structural Research PAS, PL-50422 Wroclaw, Poland;* ⓞ orcid.org/0000-0001-6088-0140

  Vitalii Boiko − *Institute of Low Temperature and Structural Research PAS, PL-50422 Wroclaw, Poland;* ⓞ orcid.org/0000-0001-6652-7890

  Tomas Murauskas − *Department of Inorganic Chemistry, Vilnius University, LT-01513 Vilnius, Lithuania*

  Piotr Solarz − *Institute of Low Temperature and Structural Research PAS, PL-50422 Wroclaw, Poland*

Complete contact information is available at:
https://pubs.acs.org/10.1021/acs.jpcc.2c00672

Author Contributions

P.G.: writing—original draft, writing—review and editing, conceptualization, formal analysis, funding acquisition, supervision, R.T.: ceramic preparation, writing—review and editing, D.K.: thermometry measurements, V.B.: TL measurements, T.M.: XPS measurements, and P.S.: luminescence decay measurements and analysis, writing—review and editing.

Notes

The authors declare no competing financial interest.

ACKNOWLEDGMENTS

REFERENCES

(1) Dereń, P. J.; Lemański, K. On tuning the spectroscopic properties of $LaAlO_3$:Pr^{3+} nanocrystallites. *J. Lumin.* **2011**, *131*, 445−448.

(2) Lukowiak, A.; Wiglusz, R. J.; Grzyb, T.; Ptak, M.; Stefanski, M.; Chiappini, A.; Strek, W. Structural and Optical Investigation of Nanocrystalline Lithium Lanthanum Praseodymium Tetraphosphate Powders. *J. Alloys Compd.* **2016**, *687*, 733−740.

(3) Watras, A.; Carrasco, I.; Pazik, R.; Wiglusz, R. J.; Piccinelli, F.; Bettinelli, M.; Deren, P. J. Structural and Spectroscopic Features of $Ca_9M(PO_4)_7$ (M = Al^{3+}, Lu^{3+}) Whitlockites Doped with Pr^{3+} Ions. *J. Alloys Compd.* **2016**, *672*, 45−51.

(4) Kolesov, R.; Xia, K.; Reuter, R.; Stöhr, R.; Zappe, A.; Meijer, J.; Hemmer, P. R.; Wrachtrup, J. Optical Detection of a Single Rare-Earth Ion in a Crystal. *Nat. Commun.* **2012**, *3*, 1029.

(5) Mao, A.; Zhao, Z.; Wang, J.; Yang, C.; Ren, J.; Wang, Y. Crystal structure and photo-luminescence of Gd$_3$Ga$_2$(Al$_{3-y}$Si$_y$)(O$_{12-y}$N$_y$):Ce^{3+} phosphors for AC-warm LEDS. *Chem. Eng. J.* **2019**, *368*, 924−932.

(6) Kowalski, R. M.; Komar, J.; Solarz, P. On the Combination of Praseodymium and Cerium, a New Concept of Improving Orange-Red Luminescence. *J. Alloys Compd.* **2020**, *848*, 156228.

(7) Nemori, H.; Matsuda, Y.; Mitsuoka, S.; Matsui, M.; Yamamoto, O.; Takeda, Y.; Imanishi, N. Stability of garnet-type solid electrolyte Li$_x$La$_3$A$_{2-y}$B$_y$O$_{12}$ (A=Nb or Ta, B=Sc or Zr). *Solid State Ionics* **2015**, *282*, 7−12.

(8) Nishiura, S.; Tanabe, S.; Fujioka, K.; Fujimoto, Y. Preparation of Transparent Ce^{3+}:GdYAG Ceramics Phosphors for White LED. *IOP Conf. Ser.: Mater. Sci. Eng.* **2011**, *18*, 102005.

(9) Antic-Fidancev, E.; Holsa, J.; krupa, J.-C.; Lemaitre-Blaise, M.; Porcher, P. Crystal fields in Pr^{3+} doped rare earth gallium garnets, RE$_3$Ga$_5$O$_{12}$:Pr^{3+}. *J. Phys. Condens. Matter* **1992**, *4*, 8321−8330.

(10) Hreniak, D.; Bettinelli, M.; Speghini, A.; Łukowiak, A.; Głuchowski, P.; Wiglusz, R. The f-f Emission of Pr^{3+} Ion as an Optical Probe for the Structural Properties of YAG Nanoceramics. *J. Nanosci. Nanotechnol.* **2009**, *9*, 6315−6319.

(11) Odziomek, M.; Chaput, F.; Lerouge, F.; Sitarz, M.; Parola, S. Highly Luminescent YAG:Ce Ultra-Small Nanocrystals, from Stable Dispersions to Thin Films. *J. Mater. Chem. C* **2017**, *5*, 12561−12570.

(12) Xie, C.; Zhao, L.; Jiang, B.; Mao, J.; Lin, Y.; Wang, P.; Wei, X.; Yin, M.; Chen, Y. Dual-activator luminescence of LuAG:Mn^{4+}/Tb^{3+} phosphor for optical thermometry. *J. Am. Ceram. Soc.* **2019**, *102*, 7500−7508.

(13) Martín-Rodríguez, R.; Valiente, R.; Polizzi, S.; Bettinelli, M.; Speghini, A.; Piccinelli, F. Upconversion Luminescence in Nanocrystals of Gd$_3$Ga$_5$O$_{12}$ and Y$_3$Al$_5$O$_{12}$ Doped with Tb^{3+}−Yb^{3+} and Eu^{3+}−Yb^{3+}. *J. Phys. Chem. C* **2009**, *113*, 12195−12200.

(14) Mallmann, E. J. J.; Sombra, A. S. B.; Goes, J. C.; Fechine, P. B. A. Yttrium Iron Garnet: Properties and Applications Review. *Solid State Phenom.* **2013**, *202*, 65−96.

(15) Inada, R.; Yasuda, S.; Tojo, M.; Tsuritani, K.; Tojo, T.; Sakurai, Y. Development of Lithium-Stuffed Garnet-Type Oxide Solid Electrolytes with High Ionic Conductivity for Application to All-Solid-State Batteries. *Front. Energy Res.* **2016**, *4*, 28.

(16) Zhong, J.; Zhuang, W.; Xing, X.; Liu, R.; Li, Y.; Liu, Y.; Hu, Y. Synthesis, Crystal Structures, and Photoluminescence Properties of Ce^{3+}-Doped Ca$_2$LaZr$_2$Ga$_3$O$_{12}$: New Garnet Green-Emitting Phosphors for White LEDs. *J. Phys. Chem. C* **2015**, *119*, 5562−5569.

(17) Xu, J.; Murata, D.; Ueda, J.; Tanabe, S. Near-Infrared Long Persistent Luminescence of Er^{3+} in Garnet for the Third Bio-Imaging Window. *J. Mater. Chem. C* **2016**, *4*, 11096−11103.

(18) Boiko, V.; Dai, Z.; Markowska, M.; Leonelli, C.; Mortalò, C.; Armetta, F.; Ursi, F.; Nasillo, G.; Saladino, M. L.; Hreniak, D. Particle Size-Related Limitations of Persistent Phosphors Based on the Doped Y$_3$Al$_2$Ga$_3$O$_{12}$ System. *Sci. Rep.* **2021**, *11*, 141 2021 111.

(19) Wang, X.; Chen, Y.; Liu, F.; Pan, Z. Solar-Blind Ultraviolet-C Persistent Luminescence Phosphors. *Nat. Commun.* **2020**, *11*, 2040 2020 111.

(20) Van den Eeckhout, K.; Smet, P. F.; Poelman, D. Persistent Luminescence in Eu^{2+}-Doped Compounds: A Review. *Materials* **2010**, *3*, 2536−2566.

(21) Cheong, W. F.; Prahl, S. A.; Welch, A. J. A Review of the Optical Properties of Biological Tissues. *IEEE J. Quantum Electron.* **1990**, *26*, 2166−2185.

(22) Hu, R.; Zhang, Y.; Zhao, Y.; Wang, X.; Li, G.; Wang, C. UV-Vis-NIR broadband-photostimulated luminescence of LiTaO$_3$:Bi^{3+} long-persistent phosphor and the optical storage properties. *Chem. Eng. J.* **2020**, *392*, 124807.

(23) Liu, L.; Shi, J.; Li, Y.; Peng, S.; Zhong, H.; Song, L.; Zhang, Y. Disguise as Fluorescent Powder: Ultraviolet-B Persistent Luminescence Material without Visible Light for Advanced Information Encryption and Anti-Counterfeiting Applications. *Chem. Eng. J.* **2022**, *430*, 132884.

(24) Głuchowski, P.; Tomala, R.; Kowalski, R.; Ignatenko, O.; Witkowski, M. E.; Drozdowski, W.; Stręk, W.; Ryba-Romanowski, W.;

(25) Pechini, M. P. Method of Preparing Lead and Alkaline Earth Titanates and Niobates and Coating Method Using the Same to Form a Capacitor. U.S. Patent 3330,697 A, 1967.

(26) Gluchowski, P.; Strek, W. Luminescence and excitation spectra of Cr^{3+}:MgAl$_2$O$_4$ nanoceramics. *Mater. Chem. Phys.* **2013**, *140*, 222.

(27) Rueden, C. T.; Schindelin, J.; Hiner, M. C.; DeZonia, B. E.; Walter, A. E.; Arena, E. T.; Eliceiri, K. W. ImageJ2: ImageJ for the next Generation of Scientific Image Data. *BMC Bioinf.* **2017**, *18*, 529.

(28) Shannon, R. D. Revised Effective Ionic Radii and Systematic Studies of Interatomic Distances in Halides and Chalcogenides. *Acta Crystallogr., Sect. A: Cryst. Phys., Diffr., Theor. Gen. Crystallogr.* **1976**, *32*, 751−767.

(29) Głuchowski, P.; Małecka, M.; Stręk, W.; Ryba-Romanowski, W.; Solarz, P. Size Effect in Novel Red Efficient Garnet Nanophosphor. *J. Phys. Chem. C* **2017**, *121*, 25561−25567.

(30) Yadav, S. K.; Uberuaga, B. P.; Nikl, M.; Jiang, C.; Stanek, C. R. Band-Gap and Band-Edge Engineering of Multicomponent Garnet Scintillators from First Principles. *Phys. Rev. Appl.* **2015**, *4*, 054012.

(31) Komar, J.; Solarz, P.; Jeżowski, A.; Głowacki, M.; Berkowski, M.; Ryba-Romanowski, W. Investigation of intrinsic and extrinsic defects in solid solution Gd$_3$(Al,Ga)$_5$O$_{12}$ crystals grown by the Czochralski method. *J. Alloys Compd.* **2016**, *688*, 96−103.

(32) Ryba-Romanowski, W.; Komar, J.; Niedźwiedzki, T.; Głowacki, M.; Berkowski, M. Excited state relaxation dynamics and up-conversion phenomena in Gd$_3$(Al,Ga)$_5$O$_{12}$ single crystals co-doped with holmium and ytterbium. *J. Alloys Compd.* **2016**, *656*, 573−580.

(33) Piątkowska, M.; Tomaszewicz, E. Solid-state synthesis, thermal stability and optical properties of new scheelite-type Pb$_{1−3x}$☐$_x$Pr$_{2x}$WO$_4$ ceramics where ☐ denotes cationic vacancies. *Mater. Lett.* **2016**, *182*, 332−335.

(34) Lertloypanyachai, P.; Pathumrangsan, N.; Sreebunpeng, K.; Pattanaboonmee, N.; Chewpraditkul, W.; Yoshikawa, A.; Kamada, K.; Nikl, M. Luminescence and Light Yield of (Gd$_2$Y)(Ga$_3$Al$_2$)O$_{12}$:Pr^{3+} Single Crystal Scintillators. *J. Cryst. Growth* **2017**, *468*, 369−372.

(35) Judd, B. R. Optical Absorption Intensities of Rare-Earth Ions. *Phys. Rev.* **1962**, *127*, 750−761.

(36) Ofelt, G. S. Intensities of Crystal Spectra of Rare-Earth Ions. *J. Chem. Phys.* **1962**, *37*, 511−520.

(37) Peacock, R. D. The Intensities of Lanthanide F--f Transitions. In *Rare Earths*; Dunitz, J. D., Hemmerich, P., Holm, R. H., Ibers, J. A., Jørgensen, C. K., Neilands, J. B., Reinen, D., Williams, R. J. P., Eds.; Springer-Verlag, 1975; pp 83−122.

(38) Quimby, R. S.; Miniscalco, W. J. Modified Judd-Ofelt technique and application to optical transitions in Pr^{3+}-doped glass. *J. Appl. Phys.* **1994**, *75*, 613−615.

(39) Guan, Y.; Tsuboi, T.; Huang, Y.; Huang, W. Concentration quenching of praseodymium ions Pr^{3+} in BaGd$_2$(MoO$_4$)$_4$ crystals. *Dalton Trans.* **2014**, *43*, 3698−3703.

(40) Lemański, K.; Bondzior, B.; Szymański, D.; Dereń, P. J. Spectroscopic properties of Gd$_x$La$_{1−x}$AlO$_3$ nanocrystals doped with Pr^{3+} ions. *New J. Chem.* **2019**, *43*, 6242−6248.

(41) Solarz, P.; Gajek, Z. Optical Transitions and Enhanced Angular Overlap Model for the Low Symmetry Europium(III) System. *J. Phys. Chem. C* **2010**, *114*, 10937−10946.

(42) Komar, J.; Lisiecki, R.; Kowalski, R.; Macalik, B.; Solarz, P.; Głowacki, M.; Berkowski, M.; Ryba-Romanowski, W. Down- and Upconversion Phenomena in Gd$_3$(Al,Ga)$_5$O$_{12}$ Crystals Doped with Pr^{3+} and Yb^{3+} Ions. *J. Phys. Chem. C* **2018**, *122*, 13061−13071.

(43) Inokuti, M.; Hirayama, F. Influence of Energy Transfer by the Exchange Mechanism on Donor Luminescence. *J. Chem. Phys.* **1965**, *43*, 1978−1989.

(44) Inkrataite, G.; Laurinavicius, G.; Enseling, D.; Zarkov, A.; Jüstel, T.; Skaudzius, R. Characterization of GAGG Doped with Extremely Low Levels of Chromium and Exhibiting Exceptional Intensity of Emission in NIR Region. *Crystals* **2021**, *11*, 673.

(45) Gharouel, S.; Marciniak, L.; Lukowiak, A.; Strek, W.; Horchani-Naifer, K.; Férid, M. Impact of Grain Size, Pr^{3+} Concentration and

Solarz, P. "Frozen" pressure effect in GGAG:Ce^{3+} white light emitting nanoceramics. *Ceram. Int.* **2019**, *45*, 21870.

Host Composition on Non-Contact Temperature Sensing Abilities of Polyphosphate Nano- and Microcrystals. *J. Rare Earths* **2019**, *37*, 812−818 August 1.

(46) Bolek, P.; Zeler, J.; Brites, C. D. S.; Trojan-Piegza, J.; Carlos, L. D.; Zych, E. Ga-Modified YAG:Pr^{3+} Dual-Mode Tunable Luminescence Thermometers. *Chem. Eng. J.* **2021**, *421*, 129764.

(47) Yuan, W.; Tan, T.; Wu, H.; Pang, R.; Zhang, S.; Jiang, L.; Li, D.; Wu, Z.; Li, C.; Zhang, H. Intense UV long persistent luminescence benefiting from the coexistence of Pr^{3+}/Pr^{4+} in a praseodymium-doped BaLu$_2$Al$_2$Ga$_2$SiO$_{12}$ phosphor. *J. Mater. Chem. C* **2021**, *9*, 5206−5216.

(48) Feng, L.; Wang, Z.; Cao, C.; Zhang, T.; Zhang, J.; Ci, Z.; Zhao, Z.; Wang, Y. Warm-White Persistent Luminescence of Lu$_3$Al$_2$Ga$_3$O$_{12}$:Pr^{3+} Phosphor. *J. Rare Earths* **2017**, *35*, 47−52.

(49) Rajfur, K.; Głuchowski, P. Design of the persistent luminescence colour of a novel Gd$_{3−x}$Tb$_x$Ga$_3$Al$_2$O$_{12}$ phosphor: synthesis methods, spectroscopic properties and mechanism. *Dalton Trans.* **2021**, *50*, 4830.

(50) Urbach, F. Zur Lumineszenz Der Alkalihalogenide: II. Messungmethoden. *Sitzungsberichte Akad. der Wissenshaften Wien* **1930**, *139*, 363.

(51) Bianconi, A.; Kotani, A.; Okada, K.; Giorgi, R.; Gargano, A.; Marcelli, A.; Miyahara, T. Many-body effects in praesodymium core-level spectroscopies of PrO$_2$. *Phys. Rev. B: Condens. Matter Mater. Phys.* **1988**, *38*, 3433.

(52) Konysheva, E. Y.; Kuznetsov, M. V. Fluctuation of surface composition and chemical states at the hetero-interface in composites comprised of a phase with perovskite structure and a phase related to the Ruddlesden-Popper family of compounds. *RSC Adv.* **2013**, *3*, 14114−14122.

(53) Baer, D. R. Guide to Making XPS Measurements on Nanoparticles. *J. Vac. Sci. Technol., A* **2020**, *38*, 031201.

(54) Kim, J.-S.; Na, C. W.; Kwak, C.-H.; Li, H.-Y.; Yoon, J. W.; Kim, J.-H.; Jeong, S.-Y.; Lee, J.-H. Humidity-Independent Gas Sensors Using Pr-Doped In$_2$O$_3$ Macroporous Spheres: Role of Cyclic Pr^{3+}/Pr^{4+} Redox Reactions in Suppression of Water-Poisoning Effect. *ACS Appl. Mater. Interfaces* **2019**, *11*, 25322−25329.

(55) Dorenbos, P.; Rogers, E. G. Vacuum Referred Binding Energies of the Lanthanides in Transition Metal Oxide Compounds. *ECS J. Solid State Sci. Technol.* **2014**, *3*, R150−R158.